Genetically Defined Subtypes of Layer 5 Somatostatin-Containing Cortical Interneurons

Rachel E. Hostetler*, Hang Hu* and Ariel Agmon(1)
Dept. of Neuroscience
West Virginia University School of Medicine and the WV Rockefeller Neuroscience Institute
* Equal contributions
(1) Corresponding author: aagmon@hsc.wvu.edu

ABSTRACT

Of the four main subclasses of inhibitory cortical interneurons, somatostatin-containing (SOM) interneurons are the most diverse. Earlier studies identified layer 1-projecting (Martinotti) cells in layer 5/6 of the X98 and the Chrna2-cre transgenic lines, and two groups of non-Martinotti cells - long-range projecting SOM cells in layers 2 and 6, and layer 4-projecting X94 cells in layers 4 and 5. Later in-vivo and ex-vivo studies described two morphological types of Martinotti cells which appear to have opposing roles in behaving animals. More recently, large-scale transcriptomic studies attempting to classify all cortical neurons by their gene expression profiles and by their morphological and electrophysiological phenotypes divided all SOM interneurons into 13 morpho-electro-transcriptomic (MET) types. It remains unclear, however, how the previously identified SOM subtypes relate to each other, and how they map onto the suggested MET classification scheme. Importantly, only a small number of Cre or Flp driver line are available to target SOM interneurons, and there are currently no genetic tools to target the majority of the proposed MET types for recording, imaging or optogenetic manipulations, severely hindering progress on understanding the roles SOM interneurons play in sensorimotor processing or in learning and memory. To begin to overcome these barriers, we undertook a systematic examination of SOM interneuron subtypes in layer 5 of mouse somatosensory cortex. We generated 4 intersectional triple-transgenic genotypes, by crossing the Sst-IRES-Flp line with 4 different Cre lines and with a dual-color reporter that labels all Cre expressing SOM cells with GFP and all other SOM cells in the same brain with tdTomato. Brains from adult mice of both sexes were retrogradely labeled by epipial dye deposits, processed histologically, and immunostained for 3 marker proteins known to be expressed in different SOM subsets. By correlating fluorescent protein expression, retrograde label and marker proteins in the same neurons, we found that Cre-expressing SOM cells in the Calb2-IRES-Cre and in the Chrna2-Cre lines, and GFP expressing neurons in the X94 line, comprise three non-overlapping SOM populations which together account for about half of all SOM cell in layer 5. Using whole-cell recordings ex-vivo, we show that they also exhibit electrophysiological properties which are distinctly different from each other. This multimodal convergence of axonal projection target, marker protein expression and electrophysiological properties strongly suggests that these three populations can be considered bona-fide SOM subtypes. Indeed, each of the three subtypes appears to map onto a unique MET type. Our findings call for a renewed effort to generate additional driver lines that can be used combinatorially to provide genetic access to the many remaining SOM subtypes and uncover their roles in cortical computations.

INTRODUCTION

In humans as in other mammals, the neocortex is where incoming sensory information relayed from the sensory periphery via the thalamus is processed and perceived, where decisions about appropriate motor responses are made, and where such motor actions are planned and controlled. While the majority of cortical neurons are excitatory, the minority inhibitory interneurons (15-20% in the rodent, (Lin et al., 1985; Beaulieu, 1993; Sahara et al., 2012) are crucial for proper neocortical function. Among other roles they balance cortical excitation, constrain pyramidal cell (PC) firing in time and space (Porter et al., 2001; Gabernet et al., 2005), control temporal precision of firing (Cardin, 2018), pace cortical rhythms (Veit et al., 2017; Antonoudiou et al., 2020; He et al., 2021), contribute to brain state modulation (Wood et al., 2017) and enhance the selectivity of sensory responses (Isaacson and Scanziani, 2011; Kepecs and Fishell, 2014). Understandably, disruption of inhibitory interneurons can lead to neurological and neuropsychiatric disorders including epilepsy, schizophrenia, autism spectrum disorders, depression, fragile X syndrome and Alzheimer's disease (Lewis et al., 2011; Marin, 2012; Inan et al., 2013; Cea-Del Rio and Huntsman, 2014; Houser, 2014; Liu et al., 2014; Soumier and Sibille, 2014; Benes, 2015; Lin and Sibille, 2015; Saiz-Sanchez et al., 2015; Fee et al., 2017; Anderson et al., 2020).

Inhibitory cortical interneurons fall into four main non-overlapping subclasses, characterized by expression of parvalbumin (PV), somatostatin (SOM), vasointestinal protein (VIP) or NDNF (Rudy et al., 2011; Tremblay et al., 2016; Feldmeyer et al., 2018; Schuman et al., 2019). This broad classification, however, conceals a multiplicity of subtypes, each with unique genetic, biochemical, morphological and electrophysiological properties, and whose precise definition is still in a state of flux (Markram et al., 2004; Petilla Interneuron Nomenclature et al., 2008; Tremblay et al., 2016; Yuste et al., 2020a). Recent large-scale transcriptomics studies have been steadily converging on a comprehensive taxonomy of inhibitory and excitatory cortical neurons, based mostly on their complement of gene transcripts (Zeisel et al., 2015; Tasic et al., 2016; Paul et al., 2017; Saunders et al., 2018; Tasic et al., 2018; Zeisel et al., 2018), with a few studies integrating transcriptomic classification with electrophysiological and morphological features (Gouwens et al., 2019; Gouwens et al., 2020; Scala et al., 2021). While preserving the major subclasses (PV, SOM, VIP, and NDNF/LAMP5), the latest and most extensive version of this taxonomy (Yao et al., 2021), based on 1.3 million cells across neocortex and hippocampus, divides these subclasses into a hierarchy of dozens of supertypes and hundreds of types and clusters.

These very large scale, effort- and data-intensive attempts at mRNA-based neuronal taxonomy, impressive as they are, have revived some old questions and controversies. What properties define a cell type (Migliore and Shepherd, 2005; Petilla Interneuron Nomenclature et al., 2008; Mukamel and Ngai, 2019; Yuste et al., 2020b; Zeng, 2022)? How do you classify neurons in which defining parameters (or gene expression profiles) appear to form a continuum, rather than fall into categorical groups (Cembrowski et al., 2016; Cembrowski and Menon, 2018; Phillips et al., 2019; Kim et al., 2020; Scala et al., 2021)? Perhaps most importantly - what level of taxonomic granularity is biologically significant? Stated differently, how does one strike a meaningful balance between "lumping" and "splitting"? Neurons in distinct transcriptomic clusters may have similar functional and morphological properties (a potential case of "over-splitting"; (Scala et al., 2021), and vice-versa, neurons in the same transcriptomic cluster may show diversity in their electrophysiology, dendritic morphology or axonal targets (a potential case of "over-

lumping"; (Peng et al., 2021). Ultimately, the utility of any neuronal classification lies in meaningfully partitioning the (enormous) set of all neurons in a given brain region into a manageable number of non-overlapping subsets, in which members of each subset are functionally equivalent and share electrophysiological properties, synaptic connectivity schemas, and patterns of activity under various conditions and during various behaviors – and can therefore be considered a single, distinct node in the cortical microcircuit. Unfortunately, a correlation between transcriptomic profiles and functional phenotypes is difficult to demonstrate. While technologies such as patch-SEQ (Cadwell et al., 2016; Fuzik et al., 2016; Lee et al., 2021) allow researchers to correlate transcriptomic profiles of single neurons with their intrinsic electrophysiological properties and their axodendritic morphology, it is much more difficult to correlate these profiles with synaptic connectivity or activity patterns during behavior, although recent studies have made some impressive inroads (Xu et al., 2020; Condylis et al., 2022). What is needed is genetic access to the diversity of subtypes, in the form of transgenic driver lines that enable expression of fluorescent proteins, excitatory and inhibitory opsins or calcium and voltage probes in specific subtypes, thus allowing different researchers to repeatedly interrogate the same subtypes employing a wide range of experimental modalities. Our goal in the current study was to develop and validate such tools for somatostatin-containing interneurons.

Of the four inhibitory subclasses, the somatostatin (SOM) group is the most diverse, as revealed by studies using SOM-specific transgenic mouse lines (Oliva et al., 2002; Halabisky et al., 2006; Ma et al., 2006; McGarry et al., 2010; Riedemann et al., 2016). In recent years SOM diversity was reinforced by the transcriptomic taxonomies. For example, combining transcriptomics (T) with morpho-electric (ME) phenotypes, a recent large-scale multimodal classification study (Gouwens et al., 2020) divided SOM interneurons into 13 "MET" types, but identified only 8 VIP types (including VIP/CCK cells), 5 PV types and 2 NDNF/LAMP5 types. This high diversity notwithstanding, the great majority of the dozens of studies which, over the past decade, examined the roles played by forebrain SOM interneurons during behaviors such as sensory processing, motor skill acquisition and associative learning, have targeted the SOM subclass en-masse, using the Sst-IRES-Cre line (Taniguchi et al., 2011). This line labels all SOM interneurons non-selectively, and even labels a small number of PV cells (Hu et al., 2013). While a few of these studies indeed observed divergent responses within the wider SOM population (Kvitsiani et al., 2013; Reimer et al., 2014; Kim et al., 2016; Anaclet et al., 2018; Yang et al., 2022), less than a handful of studies explicitly examined SOM interneuron diversity during behavior, distinguishing between SOM subsets by using subtype-specific transgenic animals, by laminar locations and/or by morphology (Munoz et al., 2017; Naka et al., 2019; Yu et al., 2019). Clearly, there is major gap between our understanding of the transcriptomic and phenotypic diversity of SOM interneurons and our ability to recognize this diversity in living brains and to selectively target specific subtypes for recording, imaging or activity manipulation. Here we begin to close this gap by applying and validating intersectional approaches for gaining access to distinct subtypes of SOM interneurons.

RESULTS

Targeting subtypes by intersectional genotypes

To develop genetic tools for accessing distinct subtypes of SOM interneurons, we searched for available mouse driver lines in which Cre recombinase was co-expressed with marker genes for distinct transcriptomic SOM groups (Tasic et al., 2018). We selected 4 such lines: Calb2-IRES-Cre (Taniguchi et al., 2011), shown to label calretinin-containing SOM cells (Taniguchi et al., 2011; He et al., 2016; Nigro et al., 2018); Chrna2-Cre (Leao et al., 2012), shown to label hippocampal O-LM interneurons and also a subset of L5 SOM cells expressing the $\alpha 2$ nicotinic receptor subunit (Hilscher et al., 2017); Calb1-IRES2-Cre (Daigle et al., 2018), in which Cre is co-expressed with calbindin, a marker for SOM subsets (Kawaguchi and Kubota, 1997; Ma et al., 2006) and Pdyn-IRES-Cre (Krashes et al., 2014), co-expressing Cre with prodynorphin. We selected the latter line since antibodies to preprodynorphin label a subset of middle-layer SOM cells (Sohn et al., 2014) and we were looking for a line which will target the X94 (non-Martinotti) SOM subtype in L4/5 (Ma et al., 2006). As did previous studies (He et al., 2016; Nigro et al., 2018), we recognized the need for intersectional genetics to refine the specificity of reporter expression, but chose a novel approach: we crossed each Cre line with the Sst-Flp line and the combinatorial RC::FLTG reporter (Plummer et al., 2015), resulting in triple-transgenic progeny in which the Cre-expressing subset of SOM cells expressed GFP while all other SOM cells (but no other cells) expressed tdTomato (Fig. 1A). For convenience, we will refer to the SOM subsets expressing GFP in the 4 intersectional genotypes above as Calb2, Chrna2, Calb1 and Pdyn cells, respectively.

We characterized the 4 intersectional genotypes by processing, imaging and analyzing brains from 3-6 animals per genotype, of both sexes, 1-5 (typically 2-3) months old. Fixed brains were cut into 30 μm sections and 4 sections per brain, 120 μm apart through the somatosensory cortex, were imaged on a confocal microscope. Representative sections from each genotype are illustrated in Fig. 1A. In each brain we counted the number of GFP-expressing and tdTomato-expressing cells by layer. Counts were normalized both to all SOM cells (GFP+tdTomato) counted in each animal and to all SOM cells counted in each layer, and descriptive statistics compiled (Table 1; Fig. 1B, upper and lower panels, respectively). The same animals were also used for the retrograde labeling and immunostaining experiments described below. When averaged over all 4 genotypes, about 15% of all SOM cells were found in Layer (L) 2/3, 10% in L4, 50% in L5 and 25% in L6. Calb2 cells comprised 8% of all SOM cells. They were found mostly in L2/3, where they represented nearly 40% of all SOM cells, with a smaller population in L5 and minor populations in L4 and 6. The Chrna2 group comprised 13% of all SOM cells, virtually all straddling the L5/6 boundary, comprising ~20% of L5 and ~10% of L6 SOM cells. Calb1 cells were 50% of all SOM interneurons; they made up 40-80% of SOM cells in all layers, with the lowest percentage in L4. Lastly, Pdyn cells were slightly less than half of all SOM cells, making up 75% of SOM cells in L4 and about half of SOM cells in L2/3 and L5, with a small number in L6. Our counts for the Calb1 and Calb2 subsets are in excellent agreement with previous counts of the same genotypes (Nigro et al., 2018).

TABLE 1	L2/3	L4	L5	L6	All layers
Calb2 (N=4)	36.1% (0.02)	6.6% (0.01)	4.8% (0.0)	2.6% (0.0)	7.8% (0.02)
Chrna2 (N=6)	0.2% (0.0)	0.0% (0.0)	21.7% (0.01)	8.8% (0.0)	13.4% (0.01)
Calb1 (N=4)	83.2% (0.01)	38.3% (0.01)	63.9% (0.02)	60.3% (0.02)	50.4% (0.03)
Pdyn (N=3)	51.8% (0.02)	75.5% (0.0)	54.7% (0.05)	14.9% (0.01)	46.7% (0.08)

Table 1. Average fractions of GFP+ cells, normalized per layer, in each of the intersections. Standard deviations (non-normalized) are in parentheses.

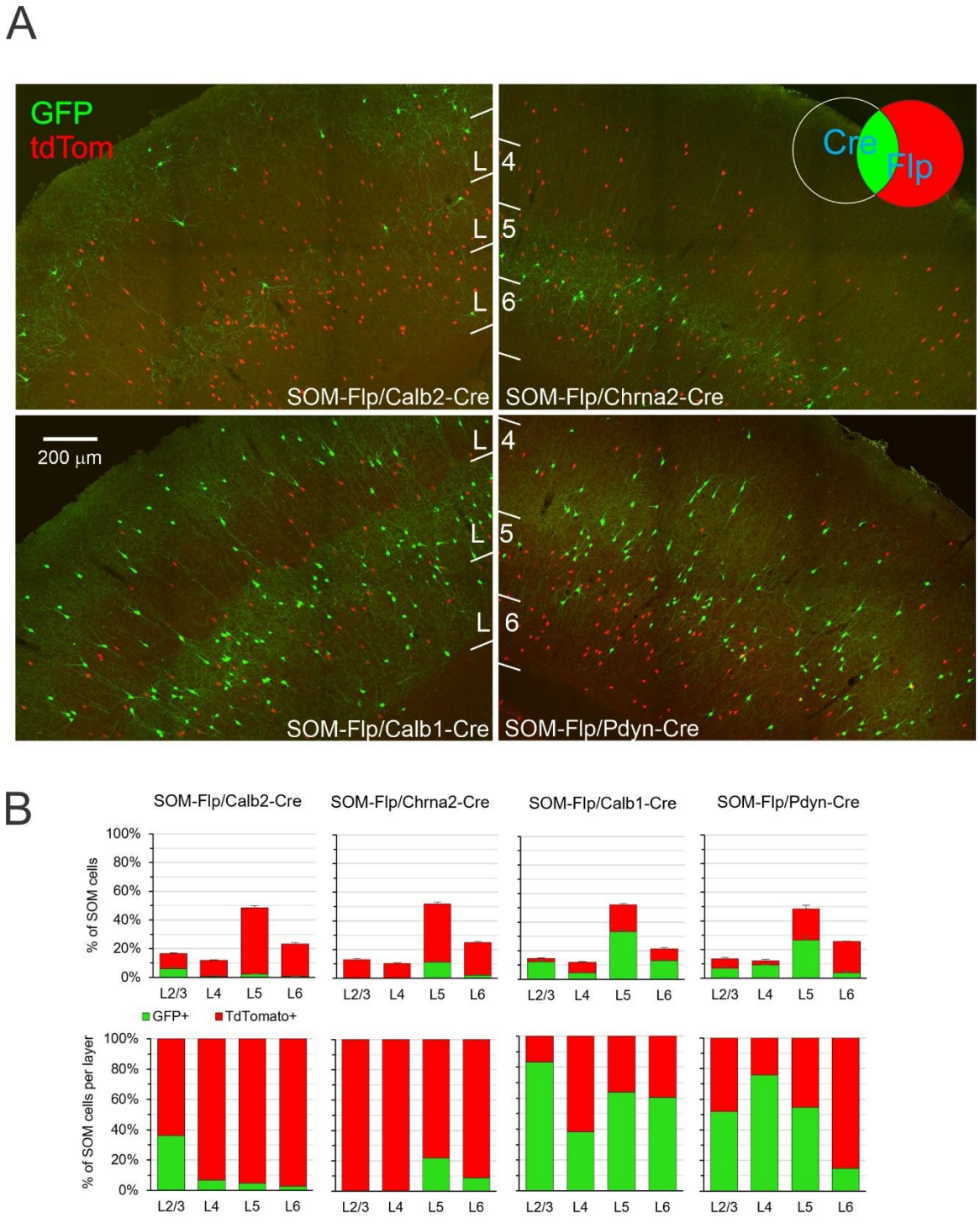

Figure 1. **Fluorescent reporter expression in the 4 intersectional genotypes**. A**.** Projections of confocal Z-stacks taken with a 20x objective of sections from the 4 genotypes. Color channels were adjusted individually. Venn diagram in upper right illustrates the combinatorial logic of the reporter. **B.** Fractions of TdTomato+ and GFP+ cells per layer in each of the intersections. N=4 mice for Calb2, N=6 mice for Chrna2, N=4 mice for Calb1, and N=3 for Pdyn. Error bars are SE.

Characterizing SOM subtypes by their L1 projection

SOM interneurons with radially ascending axons projecting to L1 are historically referred to as Martinotti cells (Kawaguchi and Kubota, 1996). Not all SOM interneurons, however, are L1-projecting; several important groups do not terminate in L1 and are collectively referred to as non-Martinotti (Tremblay et al., 2016). There is no quantitative estimate to-date on the proportion of anatomically verified Martinotti vs non-Martinotti SOM cells in the mouse cortex. To distinguish between Martinotti and non-Martinotti cells, we retrogradely labeled SOM neurons by placing a Fast Blue (FB)-infused filter paper on the pial surface, 24 hours prior to fixing the brains by transcardial perfusion (Ramos-Moreno and Clasca, 2014). FB-labeled cells were then counted by visual inspection of 10-15 optical planes through each tissue section. To validate this approach as a reliable method for labeling L1-projecting but not non-L1-projecting cells, we performed retrograde labeling in 3 X98 and 3 X94 genotypes, in which GFP-expressing SOM cells are L1- and L4- projecting, respectively (Ma et al., 2006). Overall, 79±10% (mean±SD) of all X98 cells, but only 14±6% of all X94 cells (8% in L4) were FB-labeled, consistent with their distinct axonal projection targets.

A confocal projection through a representative section from a retrogradely labeled Pdyn brain is illustrated in Fig. 2A, with the full cortical depth shown in the left panels and 4 selected ROIs (from L2/3-L6) magnified in the right panels. As seen in Fig. 2A, the majority of the FB-labeled cells in L2/3 and in L5 exhibited pyramidal morphology, and were most likely pyramidal cells labeled via their axonal terminations or dendritic tufts in L1. In contrast, L4 and L6 were mostly devoid of label, as excitatory neurons in these layers rarely extend dendrites or axons to L1 (Thomson, 2010; Wang et al., 2018). In a small number of cases, large numbers of neurons in L4 were found to be retrogradely labeled; these brains also showed signs of damage to the pial surface and diffusion of dye to L2/3, and were excluded from analysis. Notably, a thin layer of cells abutting the subcortical white matter, in L6B (also referred to as L7), were found to be brightly labeled, as previously observed after pial dye deposits (Mitchell and Cauller, 2001; Ramos-Moreno and Clasca, 2014). This strong label in the deepest cortical layer was an indication that the 24 hr survival time in our experiments was sufficient to retrogradely label any cortical neuron with an axonal projection in L1.

In each section we characterized each GFP-expressing or tdTomato-expressing cell as either FB+ or FB-. The fraction of FB+ cells in each genetic subset is quantified by layer in Fig. 2B, both as a fraction of all cells of this subset (upper panels) and normalized by layer (lower panels; Table 2). The majority of Calb2 and Chrna2 cells were FB+ (70 and 90%, respectively), while in the Calb1 and Pdyn subsets the majority of cells in L2/3 and L5 were FB+, but most cells in L4 and 6 were not. When all SOM cells (both GFP and tdTomato-expressing) were pooled across all 4 genotypes, the majority (80 and 60%, respectively) were retrogradely labeled in L2/3 and L5, but only ~20% and 40%, respectively, in L4 and L6. Out of all SOM cells in all layers, 54±5% (mean±SD; N=17) were retrogradely labeled and therefore were bona-fide Martinotti cells. This fraction varied by layer, from 80% in L2/3 to 60% in L5, 40% in L6 and <20% in L4.

TABLE 2	L2/3	L4	L5	L6	All layers
Calb2-Cre SOM (N=4)	78.0% (0.08)	65.5% (0.02)	63.2% (0.06)	33.2% (0.01)	70.5% (0.06)
Chrna2-Cre SOM (N=6)	0.0% (0.0)	-	93.8% (0.06)	71.1% (0.04)	89.9% (0.04)
Calb1-Cre SOM (N=4)	82.2% (0.02)	31.0% (0.01)	73.3% (0.03)	35.4% (0.01)	64.2% (0.05)
Pdyn-Cre SOM (N=3)	80.8% (0.03)	13.6% (0.01)	51.9% (0.01)	44.2% (0.01)	47.7% (0.02)
All SOM cells (N=17)	80.3% (0.01)	17.9% (0.01)	61.3% (0.04)	40.0% (0.01)	54.0% (0.05)

Table 2. Average percentages of FB+ GFP cells, normalized per layer, in each of the intersections, and the fraction of total FB+ SOM cells (both GFP+ and TdTomato+) in all genotypes. Standard deviations (non-normalized) are in parentheses.

Characterizing SOM subtypes by their protein marker expression

In addition to retrograde labeling, we characterized the intersectional SOM subsets by immunostaining sequential sections (N=3 brains per genotype) against three proteins known to be expressed by SOM interneurons in the mouse: calretinin (CR, product of the Calb2 gene), neuropeptide Y (NPY) and calbindin (CB, product of the Calb1 gene) (Xu et al., 2010). Representative stained sections are shown in Fig. 3A.

The number of CR+, NPY+, or CB+ cells within each subset is quantified by layer for each antibody in Fig. 3B, both as a fraction of all cells in the subset (upper panels) and normalized by layer (middle panels). The precise numbers are provided in Table 3. In the Calb2 subset, a large majority of cells (55-90%, depending on layer; 73% of all) were CR+, as expected, and an even larger fraction (>80%) were NPY+, suggesting that most Calb2 SOM cells expressed both CR and NPY, as previously noted in the cingulate cortex (Riedemann et al., 2016). The majority of Calb2 SOM cells were also CB+ (~60%). In contrast, the great majority (>90%) of Chrna2 SOM cells expressed neither CR nor NPY, indicating that the Calb2 and Chrna2 subsets are distinct populations with little or no overlap. In the Calb1 and Pdyn subsets, about half of the cells in L2/3 expressed CR and a similar fraction expressed NPY, with almost no CR expression but varying levels of NPY expression in other layers. When SOM cells (both GFP and tdTomato-expressing) were pooled across all genotypes (Fig. 3B, lower panels), at least 50% of SOM cells in layer 2/3 were CR+, NPY+, and CB+ (markers tested individually). In L4-6, <10% of SOM cells were positive for CR and <40% for NPY or CB.

Figure 2. **Retrograde FB labeling. A.** Example section from a retrogradely labeled Pdyn2 mouse. Image is a projection of a Z stack taken with a 20x objective; color channels were adjusted individually. Small scale bar is 10 µm. **B.** Fractions of FB+ labeled GFP cells per layer, for each of the genotypes. Error bars are SE. Number of animals as in Fig. 1. Plots at the far right show cumulative fraction of FB+ cells out of all SOM cells in all genotypes, N=17 mice.

A

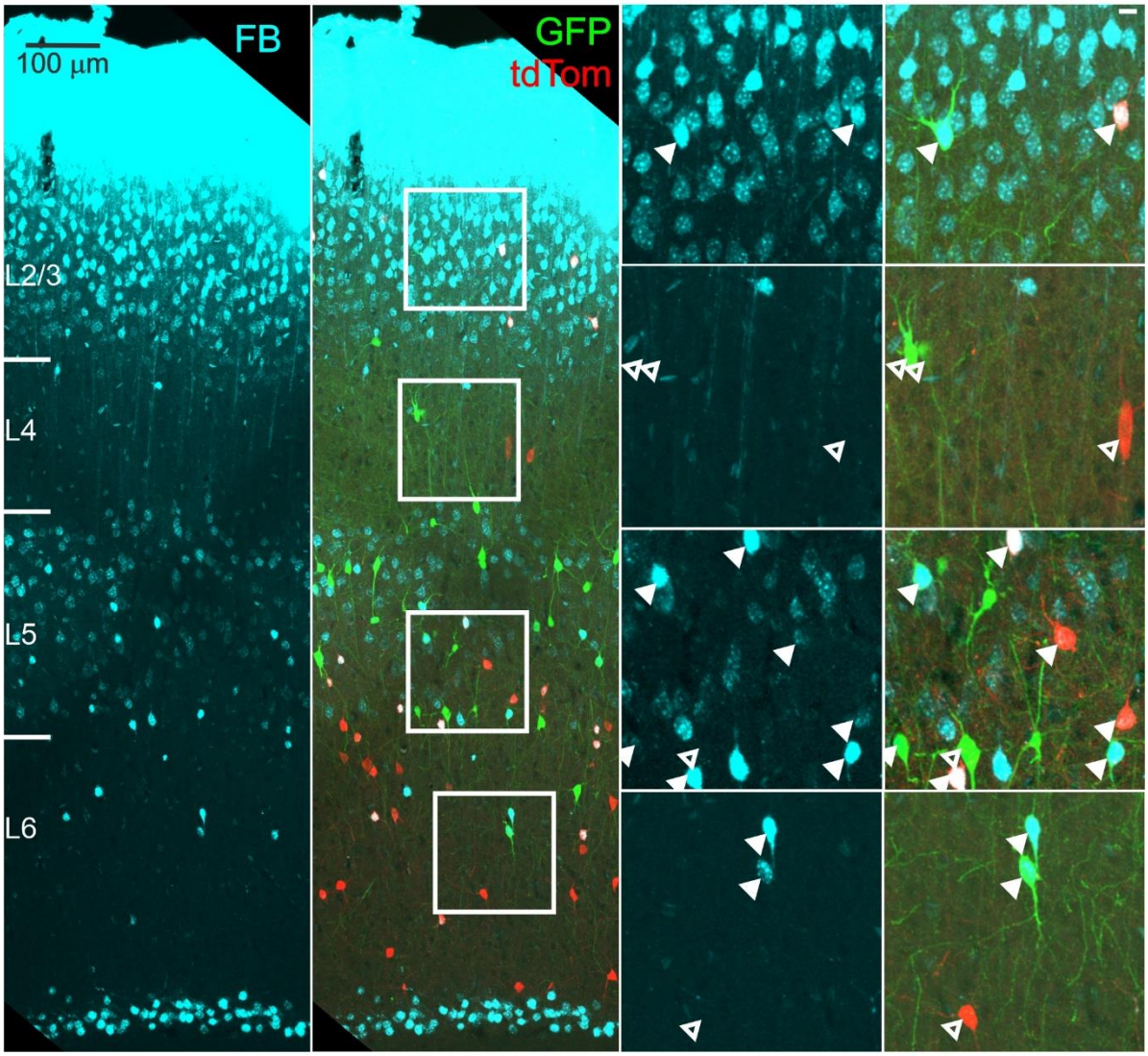

B

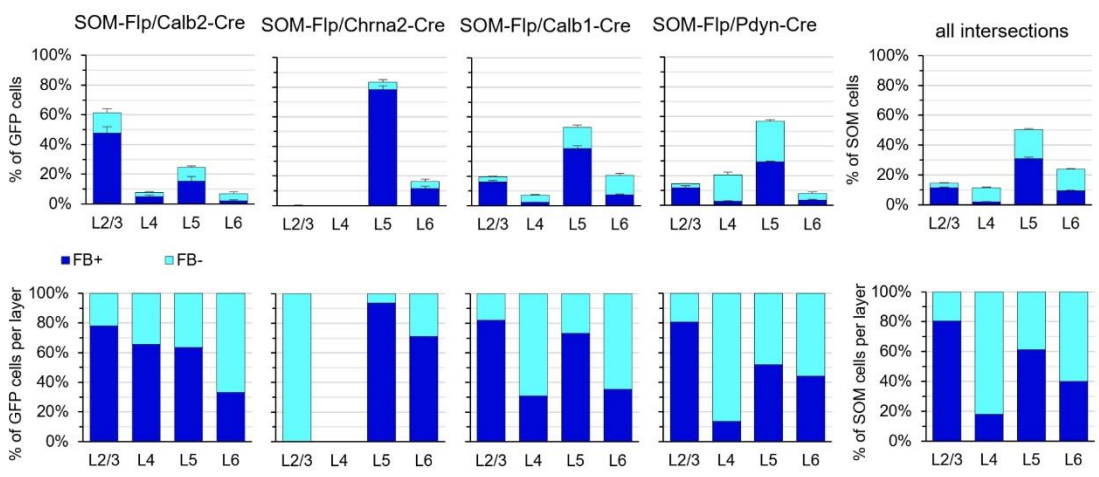

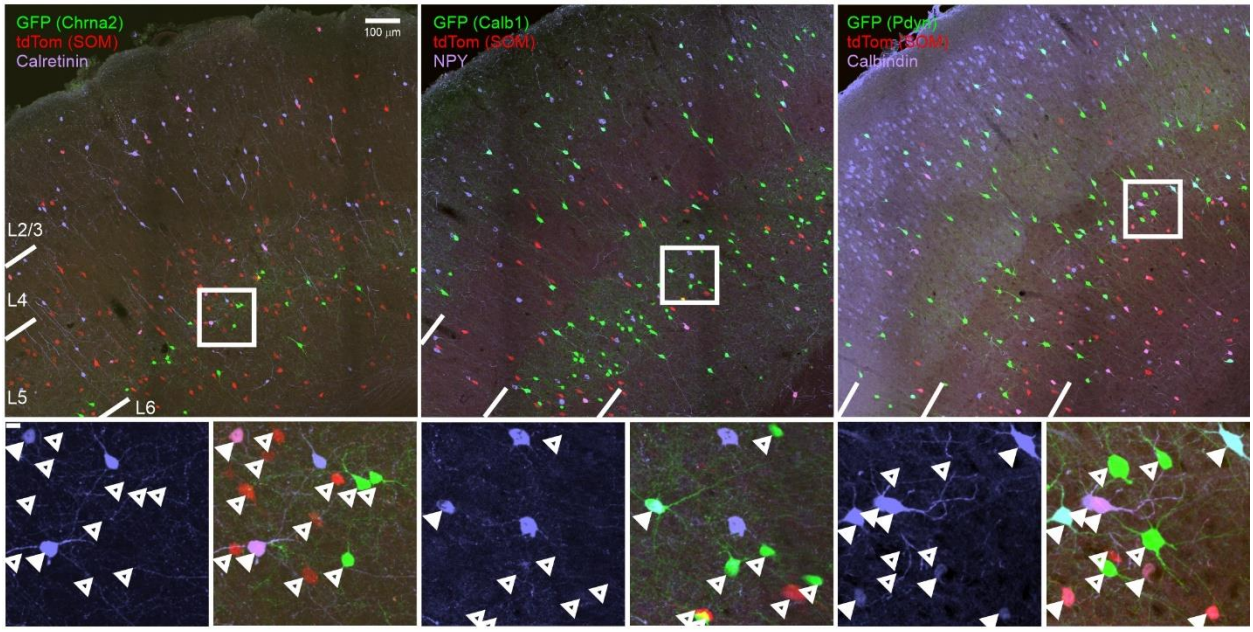

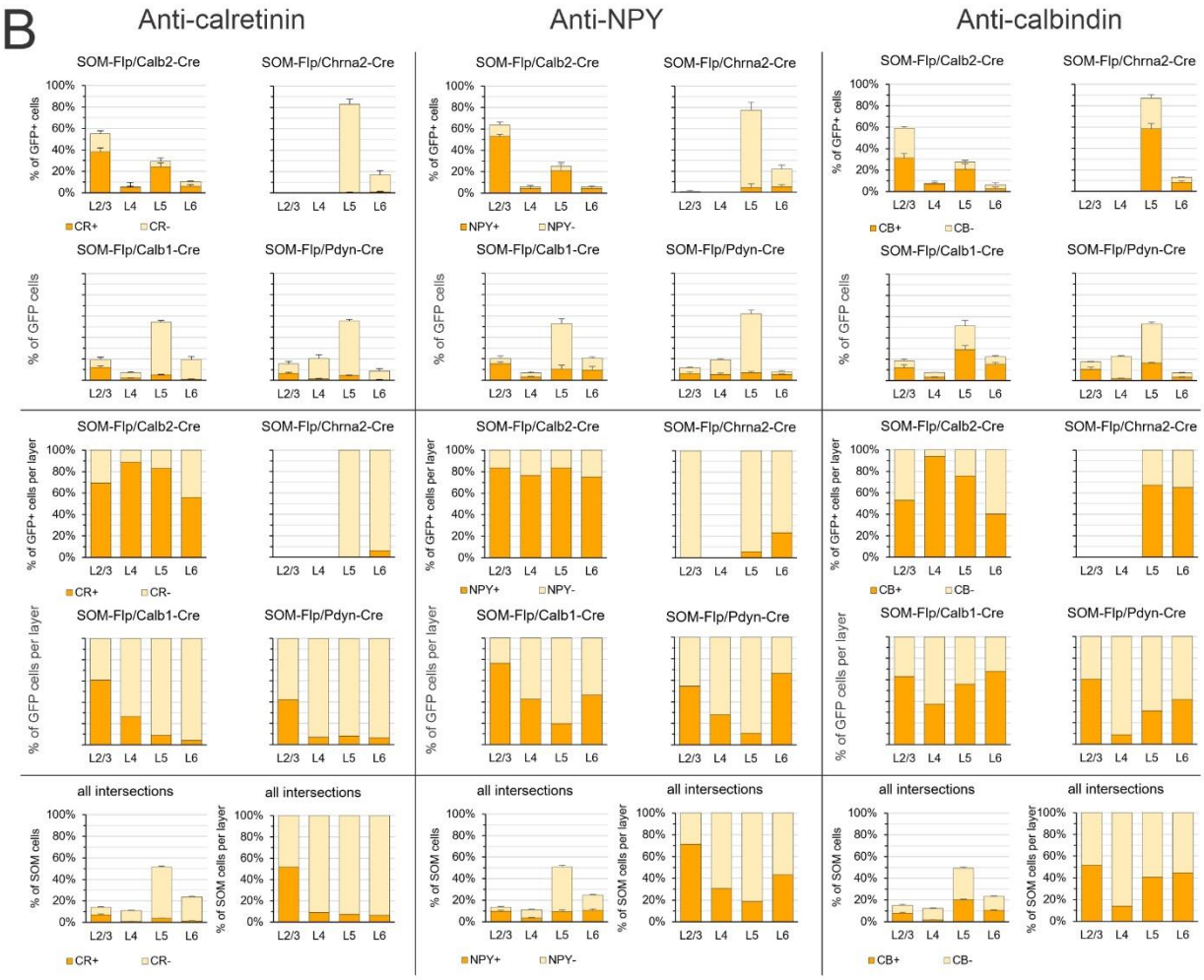

Figure 3. **A. Left,** CR immunostaining on SOM-Flp/Chrna2-Cre tissue. **Middle,** NPY immunostaining on SOM-Flp/Calb1-Cre tissue. **Right,** CB immunostaining on SOM-Flp/Pdyn-Cre tissue. All images are projections of Z stacks, taken with a 20x objective. Color channels were adjusted individually. Scale bars are 100 and 10 µm. **B,** Percentages of CR, NPY, and CB immunostained cells per GFP cells in each layer, for each of the genetic crosses, normalized for all GFP cells (top panels) or for all GFP cells in the layer (middle panel. Error bars are standard error. N=3 mice for each of the genotypes. Bottom panels, Percentages of FB+ labeling of all SOM cells (GFP+ and TdTomato+) in all animals, N=17 mice.

TABLE 3	L2/3	L4	L5	L6	All layers
Calb2					
CR+ (N=3)	69.3% (0.06)	88.9% (0.08)	83.2% (0.06)	55.9% (0.03)	73.1% (0.08)
NPY+ (N=3)	83.4% (0.04)	76.5% (0.03)	83.5% (0.11)	75.0% (0.03)	82.5% (0.15)
CB+ (N=3)	53.0% (0.07)	93.9% (0.04)	75.8% (0.09)	40.4% (0.03)	61.5% (0.01)
Chrna2					
CR+ (N=3)	0.0% (0.0)	0.0% (0.0)	0.5% (0.01)	6.0% (0.01)	1.4% (0.01)
NPY+ (N=3)	0.0% (0.0)	0.0% (0.0)	5.6% (0.06)	23.3% (0.03)	9.4% (0.08)
CB+ (N=3)	0.0% (0.0)	0.0% (0.0)	67.4% (0.08)	64.9% (0.02)	67.1% (0.06)
Pdyn					
CR+ (N=3)	42.3% (0.02)	7.0% (0.01)	8.0% (0.01)	6.1% (0.01)	13.0% (0.03)
NPY+ (N=3)	54.6% (0.02)	28.1% (0.02)	10.9% (0.02)	66.3% (0.01)	23.5% (0.06)
CB+ (N=3)	60.6% (0.04)	8.7% (0.01)	31.1% (0.01)	41.6% (0.01)	32.0% (0.03)
Calb1					
CR+ (N=3)	61.0% (0.03)	26.4% (0.01)	8.9% (0.01)	4.0% (0.01)	19.2% (0.04)
NPY+ (N=3)	76.2% (0.03)	42.5% (0.01)	19.7% (0.07)	46.3% (0.06)	38.0% (0.16)
CB+ (N=3)	62.9% (0.05)	27.4% (0.01)	55.9% 0.07)	67.9% (0.03)	58.6% (0.10)
All genotypes					
CR+ (N=12)	51.5% (0.02)	9.0% (0.01)	7.4% (0.01)	6.4% (0.0)	13.6% (0.03)
NPY+ (N=12)	71.4% (0.03)	30.6% (0.02)	18.7% (0.05)	43.3% (0.03)	33.3% (0.10)
CB+ (N=12)	51.6% (0.02)	13.8% (0.01)	40.5% (0.03)	44.5% (0.02)	39.9% (0.05)

Table 3. Average fractions of CR+, NPY+, and CB+ GFP cells, normalized per layer, in each of the genotypes. Bottom rows show cumulative fractions over all genotypes of antibody-positive cells out of all SOM cells. Standard deviations (non-normalized) are in parentheses

Multidimensional characterization of SOM subtypes

Since retrograde and immunocytochemical labeling was done on the same brains, we could relate the genetic identity of a neuron (as one of the 4 genetic subsets) both to its axonal projection and to its protein marker expression. To convey these multi-dimensional data graphically, we present them as "sunburst charts" (Figure 4). Each row of 3 sunbursts represents a genetically defined SOM subset (Calb2, Chrna2, Calb1 or Pdyn, N=3 each); each plot represents cell counts normalized to all SOM cells, averaged over the 3 brains, from all sections immunolabeled for one marker protein (CR, NPY or CB). Each sunburst consists of 4 concentric rings, each representing 100% of all SOM neurons; each color sector represents a subset whose fractional size is proportional to the angle subtended by the sector. From inside out, the rings represent cortical layer, fluorescent protein expression (green or red for GFP or tdTomato, respectively), FB labeling (dark and light blue for FB positive and negative, respectively) and immunostaining result (dark and light tan for antibody positive and negative, respectively). Each sector in the inner ring is progressively split two-way three times, ending with 32 sectors in the outer ring, each representing the fraction of SOM cells with a unique combination of laminar position, fluorescent protein expression, FB label and antibody staining status.

As illustrated in Fig. 4, Calb2 SOM cells (green sectors) were located mostly in L2/3, with a smaller population in L5. In both layers most Calb2 cells were L1-projecting (dark blue sectors) and expressed CR, NPY, and CB (dark tan sectors). Chrna2 SOM cells were located mainly in L5 with a small number in L6, and nearly all were L1-projecting. They expressed CB but, unlike Calb2 cells, almost never NPY or CR, and therefore these two genetic subsets are non-overlapping SOM populations. Pdyn SOM cells were located in all layers, comprising about 3/4 of all SOM cells in L4 and half of all SOM cells in L2/3 and L5. Most of the Pdyn SOM cells in L2/3 were L1-projecting, as indeed were most SOM cells in this layer; however only about half of those in L5 and nearly none in L4 were L1-projecting, consistent with the location of L4-targeting X94 SOM cells, which are the majority of SOM cells in L4 and a large population in L5 (Ma et al., 2006; Xu et al., 2013; Naka et al., 2019). That X94 cells in L4 and L5 were included in the Pdyn subset was also suggested by the fact that the majority of Pdyn SOM cells in L2/3 were positive for each of the 3 protein markers, but nearly none of those in L4 or of the FB- sector in L5 were immunopositive, consistent with the known absence of any of the marker proteins in X94 cells. Lastly, Calb1 SOM cells comprised the majority of SOM cells in L2/3, L5 and L6, and in L2/3 and L5 the majority of them were L1-projecting. Marker protein expression in this subset resembled that in the Pdyn subset, with most L2/3 cells positive for all 3 markers, while in L4 and L5 the majority of Calb2 cells negative for FB were also immunonegative. We conclude from these data that the Calb2 and Chrna2 SOM subsets are small, relatively homogeneous and distinct groups: both are L1-projecting and express CB, but the majority of the former reside in L2/3 with a small population in L5, whereas the latter reside exclusively in L5/6. Moreover, the majority of the Calb2 cells express CR and NPY, while Chrna2 cells express neither. In contrast, the Pdyn and the Calb1 subsets are both large (each comprising about or close to 50% of all SOM interneurons) and non-homogeneous, and most likely overlap to some extent with each other and with the other two subsets. Both contain L1-projecting cells in L2/3, most of which express all 3 markers, and also contain L1-projecting cells in L5, most of which express CB. The Pdyn group encompasses the majority of L4 SOM cells, most of which are not L1-projecting and do not express any marker, and about half of its constituent cells in L5/6 are also non-L1-projecting cells which do not express CR or CB. The Calb1 group has fewer

members in L4 but more members in L6, and the great majority of its L5/6 members are L1-projecting and/or express CB.

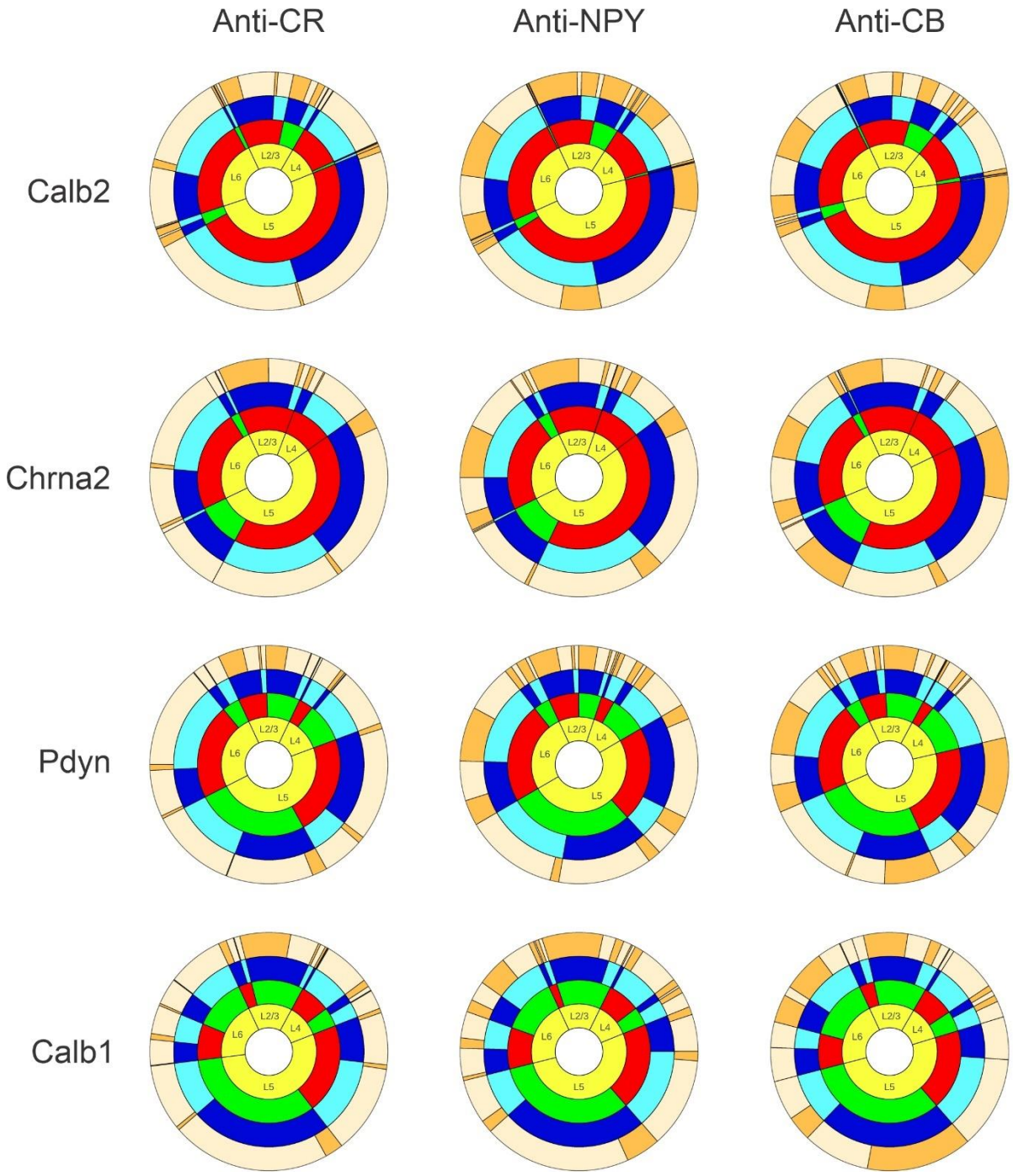

Figure 4. Sunburst plots representing fractional counts of the combined label (fluorescent protein, FB and antibody) of SOM cells in each genotypes for each antibody. N=3 per genotype. See text for detailed explanation of sunburst plots.

Electrophysiological characterization of SOM subtypes

To characterize the SOM subsets electrophysiologically, we recorded sub- and suprathreshold responses to intracellular current steps in ex-vivo slices from GFP-expressing cells in 4 genotypes: Calb2 (N=16 cells in 9 animals), Chrna2 (N=38 cells in 21 animals), Pdyn (N=24 cells from 6 animals) and X94 (N=19 cells from 9 animals). Animals were (typically) 1-2 months old, of both sexes. We did not record from Calb1 neurons because our histological cell counts indicated that this genotype captures unselectively nearly all L1-targeting subtypes. We focused on L5 where all four subsets overlap spatially. Calb2, Chrna2 and X94 SOM cells had distinct firing patterns (Fig. 5): while all subsets exhibited pronounced spike-rate adaptation during a 600 ms suprathreshold current step, Chrna2 neurons fired a characteristic low-threshold burst at the onset of the current step, and also fired a burst upon recovery from hyperpolarization (Fig. 5A). 87% of all Chrna2 cells fired a burst, but only 13% of Calb2 cells, and no X94 did. The highest firing rate achieved at the beginning of the pulse (with maximal current intensities) was <150 Hz in Calb2 neurons, 100-200 Hz in Chrna2 neurons and 150-300 Hz in X94 cells. Input resistance was highest in Chrna2 neurons (200-800 MΩ), intermediate in Calb2 neurons (200-400 MΩ) and lowest in X94 cells (<200 MΩ). A plot of initial frequency vs input resistance (Fig. 6A) showed clear separation of the three subtypes. Unlike the homogeneous properties of these 3 subsets, Pdyn neurons exhibited two distinct firing patterns and spike waveforms: some had X94-like patterns and waveforms, and the rest resembled Chrna2 neurons (Fig. 5B), suggesting that this group is a superset which includes neurons from both the X94 and the Chrna2 subsets, consistent with our conclusions from the histological experiments.

To arrive at an unbiased classification of L5 SOM cells by their electrophysiological properties, we quantified 10 intrinsic electrophysiological parameters for each cell (resting potential, input resistance, sag, firing threshold, spike height, spike width, initial firing frequency, steady-state firing frequency, adaptation ratio, AHP) (see Methods for definitions). We then applied to this dataset two dimensionality reduction methods – principal component analysis (PCA) and discriminant function analysis (DFA) (Manly, 2005; Ma et al., 2006). PCA is agnostic to the categorical identity (genotype) of each cell; it resulted in a reasonable separation of Calb2, Chrna2 and X94 cells into 3 clusters, but with considerable overlap between Calb2 and Chrna2 (Fig. 6B). DFA is designed to maximize the separation between categorized groups, and resulted in near complete segregation of the three subtypes (Fig. 6C). By both methods, Pdyn cells were split about evenly among the X94 and the Chrna2 clusters (not shown).

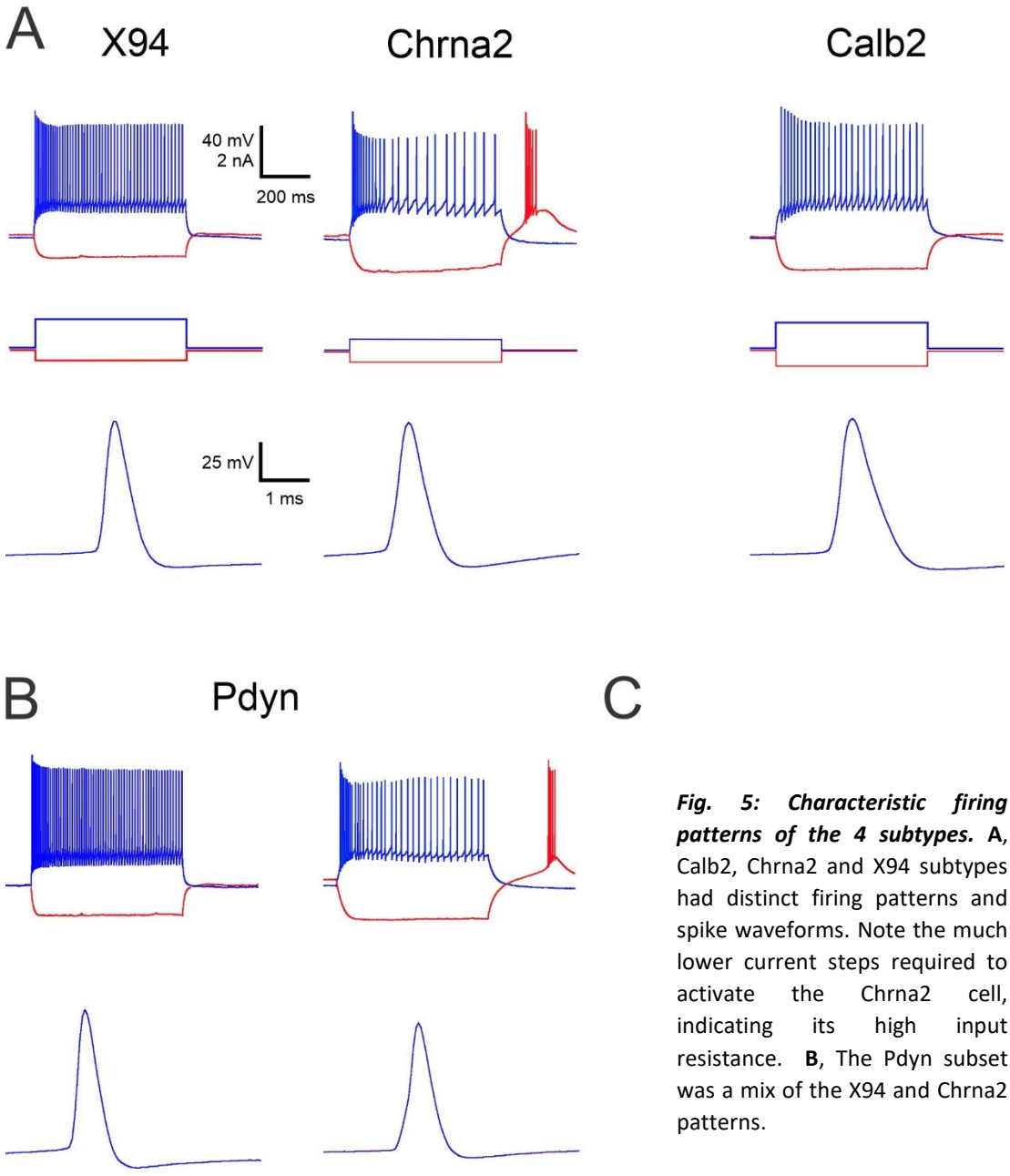

Fig. 5: Characteristic firing patterns of the 4 subtypes. **A**, Calb2, Chrna2 and X94 subtypes had distinct firing patterns and spike waveforms. Note the much lower current steps required to activate the Chrna2 cell, indicating its high input resistance. **B**, The Pdyn subset was a mix of the X94 and Chrna2 patterns.

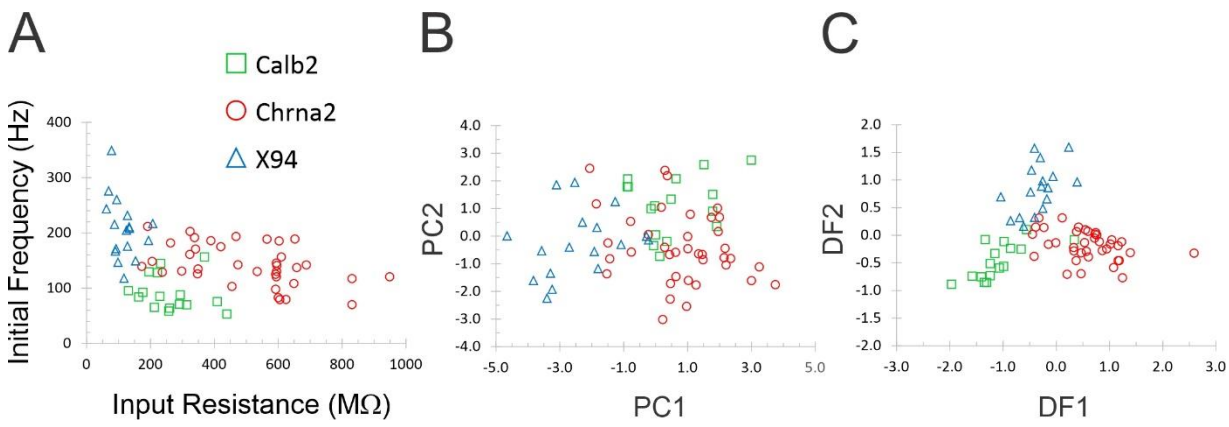

Fig. 6: Multivariate analysis of electrophysiological properties in the 2 intersectional subtypes and X94. **A**, plot of initial firing frequency vs input resistance separates the 3 subtypes. **B,** Principal component analysis leaves some overlap between Chrna2 and Calb2 point cloud. **C**, Discriminant function analysis results in near-perfect segregation of the 3 subtypes.

DISCUSSION

Classification of L5 SOM interneurons – a brief history

Our earlier study (Ma et al., 2006) identified two distinct SOM subtypes in L5, based on GFP expression in the X94 and X98 transgenic lines. These two subtypes exhibited pronounced differences in morphology, electrophysiological properties and protein markers. X98 cells were L1-targeting, had high input resistance and relatively wide spikes, about half of them fired low-threshold spike bursts and they expressed calbindin and (some) NPY. X94 cells were L4-targeting, had lower input resistance and shorter spikes, fired at high frequencies and did not express the known protein markers. A later study (Hilscher et al., 2017) described the L5 Chrna2 neurons as L1-targeting cells which fire low-threshold bursts resembling X98 cells, although no marker proteins were tested. In-vivo recordings followed by juxtacellular labeling of SOM interneurons (Munoz et al., 2017) identified, in addition to L4-targeting (non-Martinotti) cells, two morphological types of L1-projecting cells in L5 with distinct behaviorally linked activity patterns: “T-shaped”, with a single main axon extending to L1 before branching, and “fanning-out”, with multiple ascending axon collaterals and with dense arborizations in L2/3 as well as L1. Subsequent ex-vivo experiments (Nigro et al., 2018) using the Sst-flp intersection with the Calb1 and Calb2-cre lines revealed that T-shaped but not fanning-out cells fired low-threshold spikes, and that cells labeled in the Calb2 intersection were more likely to be fanning-out.

The studies above were conducted by three different laboratories using somewhat disparate methods over a protracted period of time, and left several question unanswered. For example: are the Chrna2 and Calb2, or Chrna2 and Calb1 subsets disjoint or partially overlapping? What protein markers are shared or are differentially expressed between these subsets? What are the electrophysiological properties unique to each subset? What fraction of the L5 SOM population is captured by each of them separately, and by their union? How are the intersectional genotypes related to the transgenic X94 and X98 subsets? And

finally, how do these different SOM subtypes map onto the recent transcriptomics-based classifications? Here we set out to address these questions by examining side-by-side, using identical morphological and electrophysiological methods, the five previously studied SOM-related genotypes and one novel intersection. We found a clear separation between three SOM subtypes - the Calb2, Chrna2 and X94 subtypes – which differ from each other in both categorical and quantitative properties. The Chrna2 subset resides exclusively in L5b, and the Calb2 subset is split 2:1 between L2/3 and L5/6. Both subsets are L1-projecting ("Martinotti") neurons and express calbindin, but unlike Chrna2 cells, most Calb2 cells also express calretinin and NPY, indicating that these two subsets are fully disjoint. These characteristics also set the two subsets apart from X94 cells, which reside in L4/5, are L4-projecting and do not express any of these protein markers. Moreover, these three genetically-defined subsets also have distinct firing patterns and non-overlapping electrophysiological parameters. These characteristics are summarized in Table 4.

TABLE 4	Laminar position	Projection target	Protein markers	Electrophysiological characteristic	Initial firing frequency	Input resistance
Chrna2	L5/6	L1	CB	Low-threshold burst	Intermediate	Very high
Calb2	L2/3, L5	L1	CB, CR, NPY	Frequency adaptation	Low	intermediate
X94	L4, L5	L4	----------	Quasi fast-spiking	High	Very low

Taken together, this multimodal correspondence of axonal target, neurochemical markers and electrophysiological properties strongly supports consideration of these 3 genetically-defined subsets as bona-fide neuronal subtypes of the SOM subclass. This, however, is only the first step in validating these subtypes. The true test of a neuronal subtype is whether it occupies a unique node in the cortical microcircuit – do members of the subtype share the same sources of synaptic inputs and the same targets of synaptic outputs, do they display similar patterns of electrical activity during specific behavioral tasks and different brain states, and do they differ in these properties from other putative subtypes. Intersectional approaches such as those we used here can now be combined with a variety of intersectional reporter lines or virus constructs (Plummer et al., 2015; He et al., 2016; Sciolino et al., 2016; Fenno et al., 2020), to express genetically-encoded sensors, opsins or fluorescent proteins in a subtype-specific manner, and to assess these subtype definitions using multiple experimental modalities: from voltage and calcium imaging in vivo, to simultaneous multiple recordings in brain slices, to detailed 3-D reconstruction of synaptic contacts at EM resolution. Lastly, precisely targeted activation and inactivation experiments are needed to establish the role of each subset in sensation, perception, behavior and cognition, and ultimately reveal the functional significance of SOM interneuron diversity.

Comparison with previous studies

Our experiments relied on several novel approaches. While two of the intersectional genotypes used here, Sst-flp;Calb1-cre and Sst-flp;Calb2-cre, have been used by previous studies (He et al., 2016; Nigro et al., 2018), this to our knowledge is the first use of the RC::FLTG reporter (Plummer et al., 2015) in the cortex. The advantage of this dual-color reporter is that it reveals both the subset of interest and all other SOM interneurons in the same brain, in different colors. This allowed us to directly quantify the prevalence of each subset within the wider SOM population. Notably, our fractional numbers for the Calb1 and Calb2

subsets are in excellent agreement with counts in a previous study (Nigro et al., 2018) which used immunocytochemistry to estimate all SOM interneurons, corroborating the validity of our method. Another advantage of this reporter is for electrophysiological recordings ex-vivo or for imaging experiments in-vivo, as both green and red cells can be visually targeted for recording or imaging in the same brain, providing an internal control.

Our study is also the first to apply retrograde labeling from an epipial dye deposit to identify L1-projecting interneurons in the mouse, although a previous study has done so in the rat (Ramos-Moreno and Clasca, 2014). L1-projeting SOM interneurons with radially ascending axons are historically referred to as Martinotti cells, and some earlier studies used Martinotti and somatostatin-containing as synonymous terms. However not all SOM interneurons are L1-projecting, as was made clear one and a half decades ago by the discovery of two major non-L1-projecting SOM subsets: the long-range-projecting, sleep-active NPY/nNOS-expressing cells in L6 and L2 (Tomioka et al., 2005; Gerashchenko et al., 2008), and L4-projecting X94 cells in L4 and L5b (Ma et al., 2006). The recent advent of large-scale, multimodal transcriptomic studies revealed additional SOM subtypes which do not project to L1. Out of 13 “MET” types defined by (Gouwens et al., 2020) based on combined transcriptomic profiles and morpho-electric phenotypes, 4 types (MET 10-13) have cell bodies in L5/6 and axonal arborization concentrated in L4-L6, with virtually no axonal projections in L1. This is in addition to MET types 1 and 8, corresponding to NPY/nNOS and X94 cells, respectively. Thus, only about half of all MET subtypes are bona-fide Martinotti cells; however, the transcriptomic studies are unable to assign precise prevalence fractions to any given type, as cells in these studies were not sampled in an unbiased manner. Our retrograde labeling results provide, for the first time, an unbiased estimate of the fraction of SOM interneurons with an axonal arbor in L1, which in our experiments was 54±5% (mean+SD; N=17). This fraction varied by layer, from 80% in L2/3 to 60% in L5, 40% in L6 and <20% in L4.

Interestingly, the previous rat study (Ramos-Moreno and Clasca, 2014) only identified 26% of SOM cells in S1 as retrogradely labeled after an epipial FB deposit, most of them in L2/3. Specifically, only 24% of L5, and none of the L6 SOM cells in the rat were retrogradely labeled. Both studies used the same dye concentration, and survival time in the rat study was 7 days, compared to 24 hours in the current mouse study. It is thus likely that the thicker pia mater in the rat restricts diffusion of dye more than in the mouse. As seen in the morphological reconstructions in (Gouwens et al., 2020), L1-projecting SOM cells in L5 and L6 have a relatively short total axonal extent in L1, compared to SOM cells in L2/3, so it may require higher dye concentrations in L1 to allow uptake of sufficient dye and to result in detectable label in the cell bodies in L5/6.

Another interesting observation that emerges from our detailed quantification of immunolabeled cells is that although Cre protein translation in the Calb1 and Calb2 driver lines is linked by the IRES sequence to translation of the endogenous gene, only a fraction of all Cre-expressing neurons (60-70%) were immunopositive for their eponymous marker protein. A previous study using the same intersectional lines (Nigro et al., 2018) reported a similar observation. This could mean that the remaining 30-40% of cells expressed both marker protein and Cre at a much lower level, sufficient to catalyze transgene recombination but too low to detect protein expression by immunocytochemistry. Alternatively, it could mean that the remaining cells expressed the marker protein in prenatal or earlier postnatal development, but lost that expression in the adult animals tested here.

How do the three SOM subtypes fit within the large-scale multimodal MET classification in (Gouwens et al., 2020)? The Calb2 subtype appears to correspond to MET type 4, based on calretinin expression and laminar position; the Chrna2 subtype appears to correspond to MET type 6, based on Chrna2 expression and laminar position; and X94 cells seem to correspond to MET type 8, based on their dense axonal arbor in L4, although in visual cortex they also extend some arborizations to L1 (Scala et al., 2019). Notably, all the MET type 8 reconstructions provided in (Gouwens et al., 2020) are of L4 or L5a cells; it is therefore not clear which MET type corresponds to L5b X94 cells. It is possible that L5b X94 cells are rare or absent in visual cortex. It is also worth pointing out that the morphological descriptors "T-shaped" and "fanning out" do not map onto unique MET types: both MET 6 and MET 7 are "T-shaped", and both MET 4 and MET 5 are "fanning out". What features separate neurons in each of these paired MET types remains to be determined.

What fraction of L5 SOM cells is accounted for by these three subtypes? Calb2 (5%) and Chrna2 (22%) are non-overlapping, and therefore together account for 27% of L5 SOM cells. To estimate the fraction of L5 X94 cells, we can assume that it is not more than the fraction of non-L1-projecting Pdyn cells in L5, or 26%. Thus, these three subtypes account for no more than half of L5 SOM cells. The remaining cells are likely MET 5 and 7 L1-targeting cells, as well as cells from MET 10-13 which are non-L1-targeting.

Limitations of the current intersectional approach

A limitation of the SOM-flp;Calb2-cre intersection is that it targets cells in both L2/3 and L5. According to (Gouwens et al., 2020), L2/3 and L5 calbindin-expressing neurons correspond to two different MET types (MET 3 and 4, respectively); however they occupy nearly identical positions on both the transcriptomic and electrophysiological multidimensional UMAP plots (their Fig. 6B). Our recordings, as those of a previous study of the same intersection (Nigro et al., 2018), were focused on L5, and it is possible that L2/3 Calb2 cells have subtly different electrophysiological properties. More importantly, the L2/3 and L5 subsets have been proposed to selectively target L2/3 and L5 pyramidal cells, respectively (Jiang et al., 2015), which may complicate the interpretation of activation or silencing experiments using this intersection. It is also possible that this intersection includes MET type 1 "chodl" cells (the NPY/nNOS long-range projection neurons), which also express calretinin but do not express calbindin (Tomioka et al., 2005; Gouwens et al., 2020). Indeed, our sunburst plots for this intersection reveal small populations of GFP-containing cells in L2/3 and L5/6 which do not express calbindin. Immunostaining against nNOS, and/or intracortical injections of FB or other retrograde tracers, should reveal if long-range nNOS cells are captured by this intersection.

As yet, we do not have a convenient genetic tool to specifically target the non-Martinotti X94 subtype, although the Pdyn subset is enriched in X94-like cells, compared to the total SOM population. A previous study targeted these GFP-expressing neurons with viral vectors that use GFP as a template for reconstituting a Cre-encoding construct (Naka et al., 2019); however GFP expression in the X94 line seems to label less than half of all X94-like neurons (Xu et al., 2013). Our observation that the Pdyn subset includes X94-like cells together with L1-projecting, calbindin-expressing neurons, raises the possibility of using a subtractive intersectional approach, by crossing this line with a Calb1-flp line (not currently available, to our knowledge) and using a Cre-on, Flp-off reporter line (or virus) to subtract cells which express calbindin. Alternatively, a new driver line can be designed based on marker genes identified in X94 neurons (Naka et al., 2019) or in the corresponding MET type 8 (Gouwens et al., 2020).

Conclusion

In conclusion, we recapitulate what was said in the Introduction: A major gap exists between our recognition of the transcriptomic and phenotypic diversity of SOM (and other) interneurons, and our ability to identify these diverse subtypes in living or ex-vivo brains and to selectively target them for recording, imaging or activity manipulations. This and previous studies using intersectional genetics (Nigro et al., 2018) were limited by the current availability of driver lines. Development and detailed characterization of a wide range of new driver lines, informed by the recent large-scale transcriptomic studies, is crucial if we are to clarify which of the transcriptomic clusters or multimodal (MET) types proposed by these studies are biologically meaningful, to decipher their position in the cortical microcircuit and to test their causal involvement during sensory perception, motor behavior and learning.

ACKNOWLEDGEMENTS

We are grateful to Qingyan Wang and Grace Jones for invaluable technical support, and to Amanda Ammer for technical help with imaging. We thank Bernardo Martinez for assistance with graphics software. The Chrna2-cre animals were generously provided by J. Josh Lawrence.

FUNDING

This study was supported by National Institutes of Health grant NS116604 to AA. Additional funding was provided by Transition Grant Support from the Office of Research and Graduate Education, WVU Health Sciences Center, and by the Program to Stimulate Competitive Research, Office of Research, WVU. REH was supported by NIH training grants GM081741 and GM132494. Confocal imaging was performed at the WVU Microscopic Imaging Facility which was supported by NIH grants GM121322, GM103434, GM103503, GM104942, and RR016440.

ETHICS STATEMENT

Animal husbandry and experimental procedures followed the Public Health Service Policy on Humane Care and Use of Laboratory Animals, and were approved by the WVU Institutional Animal Care and Use Committee. West Virginia University has a PHS-approved Animal Welfare Assurance D16-00362 (A3597-01).

COMPETING INTERESTS

The authors declare no competing interests.

METHODS

Animals: Animals used for histological experiments were 1-5 (typically 2-3) months old mice of both sexes. To label genetically distinct subsets of SOM interneurons, we crossed Somatostatin-Flp mice (JAX strain #028579) (He et al., 2016) with one of 4 Cre recombinase-expressing mouse lines: Calb2-Cre (JAX strain #010774) (Taniguchi et al., 2011), Calb1-Cre (JAX strain #028532) (Daigle et al., 2018), Chrna2-Cre (Leao et al., 2012), and Pdyn-Cre (JAX strain #027958) (Krashes et al., 2014). Dual-recombinase progeny were

then crossed with the RC::FLTG reporter line (JAX strain #026932) (Plummer et al., 2015), to create triple transgenic mice expressing tdTomato in Cre+/Flp- cells and GFP in Cre+/Flp+ cells. We also used X94 and X98 mice (JAX strains #006340 and #006334) (Ma et al., 2006) to label subsets of L4-projecting and L1-projecting SOM cells, respectively.

Retrograde labeling: Mice (age 4-23 weeks, male and female) were deeply anesthetized with isoflurane, placed in a heated stereotactic frame, and injected subcutaneously with local anesthetic (bupivacaine) and analgesic (meloxicam). The skull over the right primary somatosensory (barrel) cortex was exposed and a flap of bone (approx. 2x3 mm) outlined with a ¼ mm drill was removed. A filter paper circle, previously saturated with Fast Blue (FB, Polysciences, Warrington, PA, USA) dye (1% in distilled water) and allowed to dry, was cut to size, dipped in cortex buffer (composition: 125 mM NaCl, 5 mM KCl, 10 mM glucose, 10 mM HEPES, 2 mM CaCl2, 2 mM MgSO4), placed over the exposed pial surface, and covered with Kwik-Cast silicon sealant (World Precision Instruments). The surgical incision was then closed, and mice were allowed to recover.

Histology: Twenty-four hours after surgery, mice were deeply anesthetized with an intraperitoneal injection of Avertin and transcardially perfused with ~20 ml of room temperature saline followed by 50 ml of room temperature 4% paraformaldehyde (PFA) at 5 ml/min. Brains were removed and post-fixed in 4% PFA at room temperature for 4 hours on a shaker plate, then placed in 30% sucrose in phosphate-buffered saline (PBS) at 4°C on a shaker plate for at least 1-2 days. Brains were sectioned on a freezing microtome at -30°C in the coronal plane at a thickness of 30 µm for immunostaining (60 µm for X94 mice). Every FB-dyed tissue section in the barrel cortex was collected and every 4th section was used for immunostaining per antibody. Per mouse, 2-4 tissue sections were used per antibody.

Immunocytochemistry: Free floating fixed brain sections were blocked in 5% goat serum, 0.5% triton in PBS for 1 hour at room temperature, and then incubated in 1.25% goat serum, 0.125% triton-X in PBS with primary antibody for 48 hours at 4°C. Sections were then washed 3x with PBS and incubated in 1% goat serum, 0.1% triton in PBS with secondary antibodies for 2 hours at room temperature. Finally, sections were washed with PBS 3x and mounted with Vectashield Antifade or Prolong Diamond mounting medium. Sections stained with mouse primary antibodies were blocked in ReadyProbes “Mouse on Mouse” IgG blocking solution (Thermofisher) for 1 hour before the initial blocking step. Primary antibodies used: Rabbit anti-calretinin (Swant, 1:2000), mouse anti-calbindin (Swant, 1:500), and rabbit anti-neuropeptide Y (Immunostar, 1:2000). Secondary antibodies used: AlexaFluor647 anti-rabbit (Thermofisher, 1:1000) and AlexaFluor647 anti-mouse (Thermofisher, 1:500).

Confocal imaging and cell counts: Confocal Images of barrel cortex were taken on a Nikon A1R microscope using a 20x objective and a Z-step of 2.5 µm. Lasers at 405, 488, 561, and 640 nm were used to excite Fast Blue dye, GFP, TdTomato, and AlexaFluor647, respectively. All SOM interneurons (identified by GFP or tdTomato expression), within the cortical region underlying the FB deposit, were marked using NIS Elements (Nikon) as positive or negative for FB and for the relevant antibody by visually inspecting the full confocal Z-stack. Cortical layers were determined by neuronal shape, size, and density. Very few SOM cells were observed below L6, (“layer 7”), and these were excluded from the cell count. Only brains with successful retrograde labeling were included in the analysis; criteria for successful labeling included strong FB labeling in subplate neurons (evidence for sufficient incubation time) and nearly label-free L4 (evidence

for no uptake of dye below L1). Similar selection parameters have been used in previous studies using the same retrograde labeling method (Ramos-Moreno and Clasca, 2014).

Slice preparation: Mice were decapitated under deep isoflurane anesthesia, the brains removed and submerged in ice-cold, sucrose-based artificial cerebrospinal fluid (ACSF) containing the following (in mM): Sucrose 206, NaH_2PO_4 1.25, $MgCl_2.6H_2O$ 10, $CaCl_2$ 0.25, KCl 2.5, $NaHCO_3$ 26 and D-glucose 11, pH 7.4. Thalamocortical brain slices (Agmon and Connors, 1991; Porter et al., 2001) of somatosensory (barrel) cortex, 300-350 µm thick, were cut in same solution using a Leica VT-200 vibratome, and placed in a submersion holding chamber filled with recirculated and oxygenated ACSF (in mM: NaCl 126, KCl 3, NaH_2PO_4 1.25, $CaCl_2$ 2, $MgSO_4$ 1.3, NaHCO3 26, and D-glucose 20). Slices were incubated for at least 30 minutes at 32°C and then at room temperature until use. For recording, individual slices were transferred to a submersion recording chamber and continuously perfused with 32°C oxygenated ACSF at a rate of 2–3 ml/min.

Electrophysiological recordings: Recording were done on an upright microscope (FN-1, Nikon) under a 40X water immersion objective. For whole-cell recordings, glass micropipettes (typically 5–8 MΩ in resistance) were filled with an intracellular solution containing (in mM): K-gluconate 134, KCl 3.5, CaCl2 0.1, HEPES 10, EGTA 1.1, Mg-ATP 4, phosphocreatine-Tris 10, and 2 mg/ml biocytin, adjusted to pH 7.25 and 290 mOsm. Labeled neurons were identified visually by their fluorescence and then on a Nikon camera, and targeted for single or dual whole-cell recordings using a MultiClamp 700B amplifier (Molecular Devices, San-Jose, CA, USA). Upon break-in, cells were routinely tested by a standardized family of incrementing 600 ms-long intracellular current steps in both negative and positive directions. In post-hoc analysis, the same records were used in to extract multiple electrophysiological parameters for each cell. Data were acquired at a 20 kHz sampling rate using a National Instruments (Austin, TX, USA) ADC board and in-house acquisition software written in the LabView (National Instruments) environment. Reported intracellular voltages are not corrected for junction potential.

Post-hoc analysis: A total of 8 electrophysiological parameters were analyzed per cell. Single-spike parameters were measured at rheobase (minimal current evoking an action potential). All current steps were 600 ms long.

Electrophysiological parameters definitions:

V_{rest}: Resting potential upon break-in, with no holding current applied.

$V_{threshold}$: The voltage where dv/dt=5 V/s.

Spike height: Spike peak-$V_{threshold}$.

Spike width at half-height (SWHH): spike width measured half-way between $V_{threshold}$ and spike peak.

AHP: $V_{threshold}$ -Spike trough.

R_{in}: The slope of the I-V plot, calculated from 4-6 positive and negative subthreshold current steps, at membrane potentials up to ±15 mV from rest.

F_{max}: The steady-state firing frequency, computed as the reciprocal of the average of the last 5 ISI's in a spike train elicited by I_{max}.

I_{max}: The maximal current step applied before a noticeable reduction in spike height.

Multivariate analysis: Principal component analysis and discriminant function analysis were computed using custom routines, following (Manly, 2005). See (Ma et al., 2012) for a detailed description of the calculations.

REFERENCES

Agmon A, Connors BW (1991) Thalamocortical responses of mouse somatosensory (barrel) cortex in vitro. Neuroscience 41:365-379.

Anaclet C, De Luca R, Venner A, Malyshevskaya O, Lazarus M, Arrigoni E, Fuller PM (2018) Genetic Activation, Inactivation, and Deletion Reveal a Limited And Nuanced Role for Somatostatin-Containing Basal Forebrain Neurons in Behavioral State Control. J Neurosci 38:5168-5181. doi:10.1523/JNEUROSCI.2955-17.2018

Anderson KM, Collins MA, Kong R, Fang K, Li J, He T, Chekroud AM, Yeo BTT, Holmes AJ (2020) Convergent molecular, cellular, and cortical neuroimaging signatures of major depressive disorder. Proceedings of the National Academy of Sciences of the United States of America. doi:10.1073/pnas.2008004117

Antonoudiou P, Tan YL, Kontou G, Upton AL, Mann EO (2020) Parvalbumin and Somatostatin Interneurons Contribute to the Generation of Hippocampal Gamma Oscillations. J Neurosci 40:7668-7687. doi:10.1523/JNEUROSCI.0261-20.2020

Beaulieu C (1993) Numerical data on neocortical neurons in adult rat, with special reference to the GABA population. Brain Res 609:284-292.

Benes FM (2015) The GABA system in schizophrenia: cells, molecules and microcircuitry. Schizophrenia research 167:1-3. doi:10.1016/j.schres.2015.07.017

Cadwell CR, Palasantza A, Jiang X, Berens P, Deng Q, Yilmaz M, Reimer J, Shen S, Bethge M, Tolias KF, Sandberg R, Tolias AS (2016) Electrophysiological, transcriptomic and morphologic profiling of single neurons using Patch-seq. Nat Biotechnol 34:199-203. doi:10.1038/nbt.3445

Cardin JA (2018) Inhibitory Interneurons Regulate Temporal Precision and Correlations in Cortical Circuits. Trends Neurosci 41:689-700. doi:10.1016/j.tins.2018.07.015

Cea-Del Rio CA, Huntsman MM (2014) The contribution of inhibitory interneurons to circuit dysfunction in Fragile X Syndrome. Frontiers in cellular neuroscience 8:245. doi:10.3389/fncel.2014.00245

Cembrowski MS, Menon V (2018) Continuous Variation within Cell Types of the Nervous System. Trends Neurosci 41:337-348. doi:10.1016/j.tins.2018.02.010

Cembrowski MS, Bachman JL, Wang L, Sugino K, Shields BC, Spruston N (2016) Spatial Gene-Expression Gradients Underlie Prominent Heterogeneity of CA1 Pyramidal Neurons. Neuron. doi:10.1016/j.neuron.2015.12.013

Condylis C, Ghanbari A, Manjrekar N, Bistrong K, Yao S, Yao Z, Nguyen TN, Zeng H, Tasic B, Chen JL (2022) Dense functional and molecular readout of a circuit hub in sensory cortex. Science 375:eabl5981. doi:10.1126/science.abl5981

Daigle TL et al. (2018) A Suite of Transgenic Driver and Reporter Mouse Lines with Enhanced Brain-Cell-Type Targeting and Functionality. Cell 174:465-480 e422. doi:10.1016/j.cell.2018.06.035

Fee C, Banasr M, Sibille E (2017) Somatostatin-Positive Gamma-Aminobutyric Acid Interneuron Deficits in Depression: Cortical Microcircuit and Therapeutic Perspectives. Biological psychiatry. doi:10.1016/j.biopsych.2017.05.024

Feldmeyer D, Qi G, Emmenegger V, Staiger JF (2018) Inhibitory interneurons and their circuit motifs in the many layers of the barrel cortex. Neuroscience 368:132-151. doi:10.1016/j.neuroscience.2017.05.027

Fenno LE, Ramakrishnan C, Kim YS, Evans KE, Lo M, Vesuna S, Inoue M, Cheung KYM, Yuen E, Pichamoorthy N, Hong ASO, Deisseroth K (2020) Comprehensive Dual- and Triple-Feature Intersectional Single-Vector Delivery of Diverse Functional Payloads to Cells of Behaving Mammals. Neuron 107:836-853 e811. doi:10.1016/j.neuron.2020.06.003

Fuzik J, Zeisel A, Mate Z, Calvigioni D, Yanagawa Y, Szabo G, Linnarsson S, Harkany T (2016) Integration of electrophysiological recordings with single-cell RNA-seq data identifies neuronal subtypes. Nat Biotechnol 34:175-183. doi:10.1038/nbt.3443

Gabernet L, Jadhav SP, Feldman DE, Carandini M, Scanziani M (2005) Somatosensory integration controlled by dynamic thalamocortical feed-forward inhibition. Neuron 48:315-327. doi:10.1016/j.neuron.2005.09.022

Gerashchenko D, Wisor JP, Burns D, Reh RK, Shiromani PJ, Sakurai T, de la Iglesia HO, Kilduff TS (2008) Identification of a population of sleep-active cerebral cortex neurons. Proceedings of the National Academy of Sciences of the United States of America 105:10227-10232. doi:10.1073/pnas.0803125105

Gouwens NW et al. (2019) Classification of electrophysiological and morphological neuron types in the mouse visual cortex. Nat Neurosci 22:1182-1195. doi:10.1038/s41593-019-0417-0

Gouwens NW et al. (2020) Integrated Morphoelectric and Transcriptomic Classification of Cortical GABAergic Cells. Cell 183:935-953 e919. doi:10.1016/j.cell.2020.09.057

Halabisky B, Shen F, Huguenard JR, Prince DA (2006) Electrophysiological classification of somatostatin-positive interneurons in mouse sensorimotor cortex. J Neurophysiol 96:834-845. doi:10.1152/jn.01079.2005

He M, Tucciarone J, Lee S, Nigro MJ, Kim Y, Levine JM, Kelly SM, Krugikov I, Wu P, Chen Y, Gong L, Hou Y, Osten P, Rudy B, Huang ZJ (2016) Strategies and Tools for Combinatorial Targeting of GABAergic Neurons in Mouse Cerebral Cortex. Neuron 91:1228-1243. doi:10.1016/j.neuron.2016.08.021

He X, Li J, Zhou G, Yang J, McKenzie S, Li Y, Li W, Yu J, Wang Y, Qu J, Wu Z, Hu H, Duan S, Ma H (2021) Gating of hippocampal rhythms and memory by synaptic plasticity in inhibitory interneurons. Neuron 109:1013-1028 e1019. doi:10.1016/j.neuron.2021.01.014

Hilscher MM, Leao RN, Edwards SJ, Leao KE, Kullander K (2017) Chrna2-Martinotti Cells Synchronize Layer 5 Type A Pyramidal Cells via Rebound Excitation. PLoS Biol 15:e2001392. doi:10.1371/journal.pbio.2001392

Houser CR (2014) Do structural changes in GABA neurons give rise to the epileptic state? Adv Exp Med Biol 813:151-160. doi:10.1007/978-94-017-8914-1_12

Hu H, Cavendish JZ, Agmon A (2013) Not all that glitters is gold: off-target recombination in the somatostatin-IRES-Cre mouse line labels a subset of fast-spiking interneurons. Frontiers in neural circuits 7:195. doi:10.3389/fncir.2013.00195

Inan M, Petros TJ, Anderson SA (2013) Losing your inhibition: linking cortical GABAergic interneurons to schizophrenia. Neurobiology of disease 53:36-48. doi:10.1016/j.nbd.2012.11.013

Isaacson JS, Scanziani M (2011) How inhibition shapes cortical activity. Neuron 72:231-243. doi:10.1016/j.neuron.2011.09.027

Jiang X, Shen S, Cadwell CR, Berens P, Sinz F, Ecker AS, Patel S, Tolias AS (2015) Principles of connectivity among morphologically defined cell types in adult neocortex. Science 350:aac9462. doi:10.1126/science.aac9462

Kawaguchi Y, Kubota Y (1996) Physiological and morphological identification of somatostatin- or vasoactive intestinal polypeptide-containing cells among GABAergic cell subtypes in rat frontal cortex. J Neurosci 16:2701-2715.

Kawaguchi Y, Kubota Y (1997) GABAergic cell subtypes and their synaptic connections in rat frontal cortex. Cereb Cortex 7:476-486.

Kepecs A, Fishell G (2014) Interneuron cell types are fit to function. Nature 505:318-326. doi:10.1038/nature12983

Kim D, Jeong H, Lee J, Ghim JW, Her ES, Lee SH, Jung MW (2016) Distinct Roles of Parvalbumin- and Somatostatin-Expressing Interneurons in Working Memory. Neuron. doi:10.1016/j.neuron.2016.09.023

Kim EJ, Zhang Z, Huang L, Ito-Cole T, Jacobs MW, Juavinett AL, Senturk G, Hu M, Ku M, Ecker JR, Callaway EM (2020) Extraction of Distinct Neuronal Cell Types from within a Genetically Continuous Population. Neuron 107:274-282 e276. doi:10.1016/j.neuron.2020.04.018

Krashes MJ, Shah BP, Madara JC, Olson DP, Strochlic DE, Garfield AS, Vong L, Pei H, Watabe-Uchida M, Uchida N, Liberles SD, Lowell BB (2014) An excitatory paraventricular nucleus to AgRP neuron circuit that drives hunger. Nature 507:238-242. doi:10.1038/nature12956

Kvitsiani D, Ranade S, Hangya B, Taniguchi H, Huang JZ, Kepecs A (2013) Distinct behavioural and network correlates of two interneuron types in prefrontal cortex. Nature 498:363-366. doi:10.1038/nature12176

Leao RN, Mikulovic S, Leao KE, Munguba H, Gezelius H, Enjin A, Patra K, Eriksson A, Loew LM, Tort AB, Kullander K (2012) OLM interneurons differentially modulate CA3 and entorhinal inputs to hippocampal CA1 neurons. Nat Neurosci 15:1524-1530. doi:10.1038/nn.3235

Lee BR et al. (2021) Scaled, high fidelity electrophysiological, morphological, and transcriptomic cell characterization. eLife 10. doi:10.7554/eLife.65482

Lewis DA, Fish KN, Arion D, Gonzalez-Burgos G (2011) Perisomatic inhibition and cortical circuit dysfunction in schizophrenia. Curr Opin Neurobiol 21:866-872. doi:10.1016/j.conb.2011.05.013

Lin CS, Lu SM, Schmechel DE (1985) Glutamic acid decarboxylase immunoreactivity in layer IV of barrel cortex of rat and mouse. J Neurosci 5:1934-1939. doi:10.1523/JNEUROSCI.05-07-01934.1985

Lin LC, Sibille E (2015) Somatostatin, neuronal vulnerability and behavioral emotionality. Mol Psychiatry 20:377-387. doi:10.1038/mp.2014.184

Liu YQ, Yu F, Liu WH, He XH, Peng BW (2014) Dysfunction of hippocampal interneurons in epilepsy. Neuroscience bulletin 30:985-998. doi:10.1007/s12264-014-1478-4

Ma Y, Hu H, Agmon A (2012) Short-term plasticity of unitary inhibitory-to-inhibitory synapses depends on the presynaptic interneuron subtype. J Neurosci 32:983-988. doi:10.1523/JNEUROSCI.5007-11.2012

Ma Y, Hu H, Berrebi AS, Mathers PH, Agmon A (2006) Distinct subtypes of somatostatin-containing neocortical interneurons revealed in transgenic mice. J Neurosci 26:5069-5082. doi:10.1523/JNEUROSCI.0661-06.2006

Manly BFJ (2005) Multivariate Statistical Methods: A Primer. Boca Raton: Chapman &Hall/CRC.

Marin O (2012) Interneuron dysfunction in psychiatric disorders. Nat Rev Neurosci 13:107-120. doi:10.1038/nrn3155

Markram H, Toledo-Rodriguez M, Wang Y, Gupta A, Silberberg G, Wu C (2004) Interneurons of the neocortical inhibitory system. Nat Rev Neurosci 5:793-807. doi:10.1038/nrn1519

McGarry LM, Packer AM, Fino E, Nikolenko V, Sippy T, Yuste R (2010) Quantitative classification of somatostatin-positive neocortical interneurons identifies three interneuron subtypes. Frontiers in neural circuits 4:12. doi:10.3389/fncir.2010.00012

Migliore M, Shepherd GM (2005) Opinion: an integrated approach to classifying neuronal phenotypes. Nat Rev Neurosci 6:810-818. doi:10.1038/nrn1769

Mitchell BD, Cauller LJ (2001) Corticocortical and thalamocortical projections to layer I of the frontal neocortex in rats. Brain Res 921:68-77.

Mukamel EA, Ngai J (2019) Perspectives on defining cell types in the brain. Curr Opin Neurobiol 56:61-68. doi:10.1016/j.conb.2018.11.007

Munoz W, Tremblay R, Levenstein D, Rudy B (2017) Layer-specific modulation of neocortical dendritic inhibition during active wakefulness. Science 355:954-959. doi:10.1126/science.aag2599

Naka A, Veit J, Shababo B, Chance RK, Risso D, Stafford D, Snyder B, Egladyous A, Chu D, Sridharan S, Mossing DP, Paninski L, Ngai J, Adesnik H (2019) Complementary networks of cortical somatostatin interneurons enforce layer specific control. eLife 8. doi:10.7554/eLife.43696

Nigro MJ, Hashikawa-Yamasaki Y, Rudy B (2018) Diversity and Connectivity of Layer 5 Somatostatin-Expressing Interneurons in the Mouse Barrel Cortex. J Neurosci 38:1622-1633. doi:10.1523/JNEUROSCI.2415-17.2017

Oliva AA, Jr., Lam TT, Swann JW (2002) Distally directed dendrotoxicity induced by kainic Acid in hippocampal interneurons of green fluorescent protein-expressing transgenic mice. J Neurosci 22:8052-8062.

Paul A, Crow M, Raudales R, He M, Gillis J, Huang ZJ (2017) Transcriptional Architecture of Synaptic Communication Delineates GABAergic Neuron Identity. Cell 171:522-539 e520. doi:10.1016/j.cell.2017.08.032

Peng H et al. (2021) Morphological diversity of single neurons in molecularly defined cell types. Nature 598:174-181. doi:10.1038/s41586-021-03941-1

Petilla Interneuron Nomenclature G et al. (2008) Petilla terminology: nomenclature of features of GABAergic interneurons of the cerebral cortex. Nat Rev Neurosci 9:557-568. doi:10.1038/nrn2402

Phillips JW, Schulmann A, Hara E, Winnubst J, Liu C, Valakh V, Wang L, Shields BC, Korff W, Chandrashekar J, Lemire AL, Mensh B, Dudman JT, Nelson SB, Hantman AW (2019) A repeated molecular architecture across thalamic pathways. Nat Neurosci 22:1925-1935. doi:10.1038/s41593-019-0483-3

Plummer NW, Evsyukova IY, Robertson SD, de Marchena J, Tucker CJ, Jensen P (2015) Expanding the power of recombinase-based labeling to uncover cellular diversity. Development 142:4385-4393. doi:10.1242/dev.129981

Porter JT, Johnson CK, Agmon A (2001) Diverse types of interneurons generate thalamus-evoked feedforward inhibition in the mouse barrel cortex. J Neurosci 21:2699-2710.

Ramos-Moreno T, Clasca F (2014) Quantitative mapping of the local and extrinsic sources of GABA and Reelin to the layer Ia neuropil in the adult rat neocortex. Brain structure & function 219:1639-1657. doi:10.1007/s00429-013-0591-x

Reimer J, Froudarakis E, Cadwell CR, Yatsenko D, Denfield GH, Tolias AS (2014) Pupil fluctuations track fast switching of cortical states during quiet wakefulness. Neuron 84:355-362. doi:10.1016/j.neuron.2014.09.033

Riedemann T, Schmitz C, Sutor B (2016) Immunocytochemical heterogeneity of somatostatin-expressing GABAergic interneurons in layers II and III of the mouse cingulate cortex: A combined immunofluorescence/design-based stereologic study. J Comp Neurol 524:2281-2299. doi:10.1002/cne.23948

Rudy B, Fishell G, Lee S, Hjerling-Leffler J (2011) Three groups of interneurons account for nearly 100% of neocortical GABAergic neurons. Developmental neurobiology 71:45-61. doi:10.1002/dneu.20853

Sahara S, Yanagawa Y, O'Leary DD, Stevens CF (2012) The fraction of cortical GABAergic neurons is constant from near the start of cortical neurogenesis to adulthood. J Neurosci 32:4755-4761. doi:10.1523/JNEUROSCI.6412-11.2012

Saiz-Sanchez D, De la Rosa-Prieto C, Ubeda-Banon I, Martinez-Marcos A (2015) Interneurons, tau and amyloid-beta in the piriform cortex in Alzheimer's disease. Brain structure & function 220:2011-2025. doi:10.1007/s00429-014-0771-3

Saunders A, Macosko EZ, Wysoker A, Goldman M, Krienen FM, de Rivera H, Bien E, Baum M, Bortolin L, Wang S, Goeva A, Nemesh J, Kamitaki N, Brumbaugh S, Kulp D, McCarroll SA (2018) Molecular Diversity and Specializations among the Cells of the Adult Mouse Brain. Cell 174:1015-1030 e1016. doi:10.1016/j.cell.2018.07.028

Scala F, Kobak D, Shan S, Bernaerts Y, Laturnus S, Cadwell CR, Hartmanis L, Froudarakis E, Castro JR, Tan ZH, Papadopoulos S, Patel SS, Sandberg R, Berens P, Jiang X, Tolias AS (2019) Layer 4 of mouse neocortex differs in cell types and circuit organization between sensory areas. Nature communications 10:4174. doi:10.1038/s41467-019-12058-z

Scala F, Kobak D, Bernabucci M, Bernaerts Y, Cadwell CR, Castro JR, Hartmanis L, Jiang X, Laturnus S, Miranda E, Mulherkar S, Tan ZH, Yao Z, Zeng H, Sandberg R, Berens P, Tolias AS (2021) Phenotypic variation of transcriptomic cell types in mouse motor cortex. Nature 598:144-150. doi:10.1038/s41586-020-2907-3

Schuman B, Machold RP, Hashikawa Y, Fuzik J, Fishell GJ, Rudy B (2019) Four Unique Interneuron Populations Reside in Neocortical Layer 1. J Neurosci 39:125-139. doi:10.1523/JNEUROSCI.1613-18.2018

Sciolino NR, Plummer NW, Chen YW, Alexander GM, Robertson SD, Dudek SM, McElligott ZA, Jensen P (2016) Recombinase-Dependent Mouse Lines for Chemogenetic Activation of Genetically Defined Cell Types. Cell reports 15:2563-2573. doi:10.1016/j.celrep.2016.05.034

Sohn J, Hioki H, Okamoto S, Kaneko T (2014) Preprodynorphin-expressing neurons constitute a large subgroup of somatostatin-expressing GABAergic interneurons in the mouse neocortex. J Comp Neurol 522:1506-1526. doi:10.1002/cne.23477

Soumier A, Sibille E (2014) Opposing effects of acute versus chronic blockade of frontal cortex somatostatin-positive inhibitory neurons on behavioral emotionality in mice. Neuropsychopharmacology : official publication of the American College of Neuropsychopharmacology 39:2252-2262. doi:10.1038/npp.2014.76

Taniguchi H, He M, Wu P, Kim S, Paik R, Sugino K, Kvitsiani D, Fu Y, Lu J, Lin Y, Miyoshi G, Shima Y, Fishell G, Nelson SB, Huang ZJ (2011) A resource of Cre driver lines for genetic targeting of GABAergic neurons in cerebral cortex. Neuron 71:995-1013. doi:10.1016/j.neuron.2011.07.026

Tasic B et al. (2016) Adult mouse cortical cell taxonomy revealed by single cell transcriptomics. Nat Neurosci 19:335-346. doi:10.1038/nn.4216

Tasic B et al. (2018) Shared and distinct transcriptomic cell types across neocortical areas. Nature 563:72-78. doi:10.1038/s41586-018-0654-5

Thomson AM (2010) Neocortical layer 6, a review. Frontiers in neuroanatomy 4:13. doi:10.3389/fnana.2010.00013

Tomioka R, Okamoto K, Furuta T, Fujiyama F, Iwasato T, Yanagawa Y, Obata K, Kaneko T, Tamamaki N (2005) Demonstration of long-range GABAergic connections distributed throughout the mouse neocortex. Eur J Neurosci 21:1587-1600. doi:10.1111/j.1460-9568.2005.03989.x

Tremblay R, Lee S, Rudy B (2016) GABAergic Interneurons in the Neocortex: From Cellular Properties to Circuits. Neuron 91:260-292. doi:10.1016/j.neuron.2016.06.033

Veit J, Hakim R, Jadi MP, Sejnowski TJ, Adesnik H (2017) Cortical gamma band synchronization through somatostatin interneurons. Nat Neurosci. doi:10.1038/nn.4562

Wang Y, Ye M, Kuang X, Li Y, Hu S (2018) A simplified morphological classification scheme for pyramidal cells in six layers of primary somatosensory cortex of juvenile rats. IBRO Rep 5:74-90. doi:10.1016/j.ibror.2018.10.001

Wood KC, Blackwell JM, Geffen MN (2017) Cortical inhibitory interneurons control sensory processing. Curr Opin Neurobiol 46:200-207. doi:10.1016/j.conb.2017.08.018

Xu H, Jeong HY, Tremblay R, Rudy B (2013) Neocortical somatostatin-expressing GABAergic interneurons disinhibit the thalamorecipient layer 4. Neuron 77:155-167. doi:10.1016/j.neuron.2012.11.004

Xu S, Yang H, Menon V, Lemire AL, Wang L, Henry FE, Turaga SC, Sternson SM (2020) Behavioral state coding by molecularly defined paraventricular hypothalamic cell type ensembles. Science 370. doi:10.1126/science.abb2494

Xu X, Roby KD, Callaway EM (2010) Immunochemical characterization of inhibitory mouse cortical neurons: three chemically distinct classes of inhibitory cells. J Comp Neurol 518:389-404. doi:10.1002/cne.22229

Yang J, Serrano P, Yin X, Sun X, Lin Y, Chen SX (2022) Functionally distinct NPAS4-expressing somatostatin interneuron ensembles critical for motor skill learning. Neuron 110:3339-3355 e3338. doi:10.1016/j.neuron.2022.08.018

Yao Z et al. (2021) A taxonomy of transcriptomic cell types across the isocortex and hippocampal formation. Cell 184:3222-3241 e3226. doi:10.1016/j.cell.2021.04.021

Yu J, Hu H, Agmon A, Svoboda K (2019) Recruitment of GABAergic Interneurons in the Barrel Cortex during Active Tactile Behavior. Neuron 104:412-427 e414. doi:10.1016/j.neuron.2019.07.027

Yuste R et al. (2020a) A community-based transcriptomics classification and nomenclature of neocortical cell types. Nat Neurosci. doi:10.1038/s41593-020-0685-8

Yuste R et al. (2020b) A community-based transcriptomics classification and nomenclature of neocortical cell types. Nat Neurosci 23:1456-1468. doi:10.1038/s41593-020-0685-8

Zeisel A, Munoz-Manchado AB, Codeluppi S, Lonnerberg P, La Manno G, Jureus A, Marques S, Munguba H, He L, Betsholtz C, Rolny C, Castelo-Branco G, Hjerling-Leffler J, Linnarsson S (2015) Brain structure. Cell types in the mouse cortex and hippocampus revealed by single-cell RNA-seq. Science 347:1138-1142. doi:10.1126/science.aaa1934

Zeisel A, Hochgerner H, Lonnerberg P, Johnsson A, Memic F, van der Zwan J, Haring M, Braun E, Borm LE, La Manno G, Codeluppi S, Furlan A, Lee K, Skene N, Harris KD, Hjerling-Leffler J, Arenas E, Ernfors P, Marklund U, Linnarsson S (2018) Molecular Architecture of the Mouse Nervous System. Cell 174:999-1014 e1022. doi:10.1016/j.cell.2018.06.021

Zeng H (2022) What is a cell type and how to define it? Cell 185:2739-2755. doi:10.1016/j.cell.2022.06.031